International Journal of Heat and Mass Transfer 61 (2013) 543–553

Contents lists available at SciVerse ScienceDirect

International Journal of Heat and Mass Transfer

journal homepage: www.elsevier.com/locate/ijhmt

# Lattice Boltzmann method and large-eddy simulation for turbulent impinging jet cooling

Yue-Tzu Yang, Shing-Cheng Chang *, Chu-Shiang Chiou

*Department of Mechanical Engineering, National Cheng Kung University, Tainan 70101, Taiwan*

ARTICLE INFO

*Article history:*
Received 18 July 2012
Received in revised form 8 February 2013
Accepted 8 February 2013
Available online 15 March 2013

*Keywords:*
Lattice Boltzmann method
Vorticity-stream function
Turbulence
Large-eddy simulation
Impingement jet cooling

ABSTRACT

In this paper, a large-eddy-based lattice Boltzmann model for energy equation is proposed to simulate the heat transfer phenomena of impinging jet flow. The hydrodynamic properties of two-dimensional turbulence are obtained by solving vorticity-stream function formulation with similar lattice Boltzmann model. The simulation results of a lid-driven flow and a backward-facing flow show the validity of the present model for a closed or an open flow field. For impinging jet flows, the cooling efficiency on the surface under constant-temperature or constant-heat-flux condition is investigated. The flow is found to be laminar or turbulent depending on not only the Reynolds number but also the ratio of jet-to-surface distance to jet exit width. In the laminar jet flow, stationary vortices formed near the surface reduce the thermal diffusibility, while the transient moving vortices remove the energy from hot surface rapidly. Therefore, the cooling efficiency of a turbulent jet flow is better than that of a laminar jet flow.



## 1. Introduction

In recent years, the lattice Boltzmann method (LBM) [1,2] developed from the lattice gas cellular automata (LGCA) has been applied to many researches, especially in mesoscopic engineering and science as microfluidics [3]. As a promising method of computational fluid dynamics (CFD), LBM treats the fluid particles on a statistical level and simulates fluid flows by simplified kinetic models, which are incorporated with essential physics of microscopic processes and associated with macroscopic physical properties. Essentially, this bottom–up scheme is different from traditional CFD methods of top–down schemes, which analyze flow fields by solving macroscopic variables in the Navier–Stokes equations.

The lattice Boltzmann equation (LBE) was first proposed by McNamara and Zanetti [4]. In their work, the ensemble-average density distribution functions were introduced to substitute the Boolean operators in LGCA, so that macroscopic properties of fluid flows can be calculated by solving this velocity discrete Boltzmann equation. Similar to LGCA, LBM includes a two-step evolution of particle distribution functions, namely particle distribution "collisions" on lattice nodes and stream "propagations" from one node to all neighbors along the lattice directions. After streaming, new local properties on lattice nodes are obtained by distribution components from neighbors. The complex collision terms in the Boltzmann equation are replaced by a simplified relaxation model in the LBE, i.e. the well-known Bhatnagar–Gross–Krook (BGK) model [5]. By the Chapman–Enskog expansion [1], the lattice BGK model can be recovered to the Navier–Stokes equations successfully.

The LBM possesses advantage to implement boundaries with complex or fractal geometry [6], and has been extensively applied to various physical processes and phenomena, such as heat transfer, electric field, magnetic field, and etc. However, to simulate a turbulent flow field by LBM is still a challenge. The common methods for simulating turbulence are direct numerical simulation (DNS), Reynolds average numerical simulation (RANS), and large-eddy simulation (LES) proposed by Smagorinsky [7]. The main idea of the LES is to describe turbulence by two models of different scales, namely the large scale part solved by direct numerical calculation and the small scale part described by a turbulence model. The LES has been used to solve many turbulent problems, e.g. simple hydraulic channels [8], gas turbine combustor flow [9], buoyant jets [10], free surface [11], and heat transfer for turbulent flows [12]. By combination of the vorticity-stream function and LES, Chen [13] presented a lattice Boltzmann model to simulate turbulence. Turbulent governing equations using the vorticity-stream function equations with combination of the LES model were solved by the LBM. The traditional constraints of low Mach number and relaxation time in LBM are overcome in this model, and hence the accuracy in the simulation of turbulence is improved.

Jet impingement heat transfer is a widely studied flow configuration because of its industrial as well as fundamental importance. Numerous research scholars have examined the thermal and hydraulic characteristics of different turbulence models on impingement jet. A comprehensive study of the standard $k-\varepsilon$ model was carried out by Agarwal and Bower [14], which was

* Corresponding author. Tel.: +886 6 2757575x62245.
*E-mail address:* mr_scchang@yahoo.com.tw (S.-C. Chang).

0017-9310/$ - see front matter © 2013 Elsevier Ltd. All rights reserved.
http://dx.doi.org/10.1016/j.ijheatmasstransfer.2013.02.022

**Nomenclature**

| | |
|---|---|
| $c$ | Lattice streaming speed (m/s) |
| $C$ | Smagorinsky constant |
| $C_s$ | speed of sound (m/s) |
| $f_i$ | Stream distribution function |
| $f_i^{eq}$ | equilibrium distribution function for $f_i$ |
| $g_i$ | vorticity distribution function |
| $g_i^{eq}$ | equilibrium distribution function for $g_i$ |
| $h$ | heat transfer coefficient ($W/m^2 \cdot K$) |
| $H$ | height of impinging jet flow (m) |
| $H_1$ | height of lid-driven flow (m) |
| $H_2$ | Step height in backward-facing step flow (m) |
| $k_f$ | thermal conductivity ($W/m \cdot K$) |
| L | length of flow passageway (m) |
| Nu | Nusselt number |
| Pr | Prandtl number |
| $q$ | heat flux ($W/m^2$) |
| $q_0$ | characteristic heat flux ($W/m^2$) |
| Re | Reynolds number |
| S | strain rate |
| t | time (s) |
| $\tau_e$ | relaxation time |
| $T$ | temperature (K) |
| $v$ | velocity (m/s) |
| $V_{in}$ | inlet velocity of impinging jet flow (m/s) |
| $W$ | width of impinging jet flow (m) |
| $x,y$ | Cartesian coordinates |

*Greek symbols*

| | |
|---|---|
| $\alpha$ | thermal diffusivity ($m^2/s$) |
| $\upsilon$ | kinematic viscosity ($m^2/s$) |
| $\omega$ | vorticity (1/s) |
| $\psi$ | Stream function ($m^2/s$) |
| $\Delta x,\Delta y$ | grid spacing (m) |
| $\Delta t$ | discrete time step (s) |

*Superscripts*

| | |
|---|---|
| $\bar{\ }$ | large scale variable |
| $\rightarrow$ | vector |
| $'$ | sub-scale variable |
| $*$ | dimensionless |

*Subscripts*

| | |
|---|---|
| 0 | fluid |
| $T$ | turbulence |
| $w$ | wall |

considered being more accurate than the one equation model for compressible turbulent flow. Maveety and Hendricks [15] conducted a study for the cooling of heat-sink with jet impingement in a range of Reynolds number and dimensionless impingement distance. The best performance occurred when the Reynolds number was between 40,000 and 50,000 and when the dimensionless impingement distance was from 8 to 12. Shi et al. [16] numerically analyzed the standard $k-\varepsilon$ model and the RSM turbulence model of confined jet impingement. The numerical results have shown that impinging distance plays an important role in determining the accuracy. Five different low-Reynolds $k-\varepsilon$ turbulent models were compared in Wang and Mujumdar [17] to investigate the numerical accuracy with the experiment on confined jet impingement. They found that none of the five models was validated with the experiment. However, combing the low-Reynolds with YAP correction reduced error of the predictions. Zu and Yan [18] investigated of the performance of 7 different turbulence models to predict the thermal and flow characteristic of confined impinging jet. The SST k-$\omega$ model was suggested to a better performance on calculation efficiency and accuracy. Five different turbulence models were developed by Sharif and Mothe [19] for the prediction of heat transfer due to slot jet on plane and concave surface. Nozzle-to-distance was found to strongly affect the accuracy of the predicted Nusselt number. When the nozzle-to-distance was longer than the length of potential core, the results revealed a higher prediction. The author suggested using the RNG $k-\varepsilon$ model and the SST $k-\omega$ model to give a better prediction in the computation. Benim et al. [20] evaluated several different turbulence models for the computation of turbulent flow onto a rotational circular plate. The results revealed that the predictions of the RNG $k-\varepsilon$ model and the SST $k-\omega$ model perform as good as the simulations of anisotropic Reynolds stress models. Thirteen different turbulence models in the prediction of round-jet impingement heat transfer from an isothermal flat surface were evaluated by Herbert et al. [21]. The SST-$k-\omega$ with a transitional flow option activated was found to have the best performance. In addition, when the impingement was within the jet potential core, it gives the best performance in the prediction of the secondary peak of the surface Nusselt number.

From the above literature mentioned, it can been seen that although jet impingement has been thoroughly investigated, only a few studies attempt to conduct the numerical simulation for a jet impingement using lattice Boltzmann method and large-eddy simulation. In addition, to our knowledge, there are few studies concentrating on the topic of turbulent impingement cooling using LBM/LES. In this study, Chen's method [13] is adopted and extended to energy equation to study the transport phenomena of impinging jet flows, which are employed in a wide variety of applications in engineering, such as surface cleaning, heating, and cooling of electronic components. The previous work [22] studied the thermal effects of a radiator with an impinging jet flow, and indicated that the heat transfer efficiency can be enhanced by

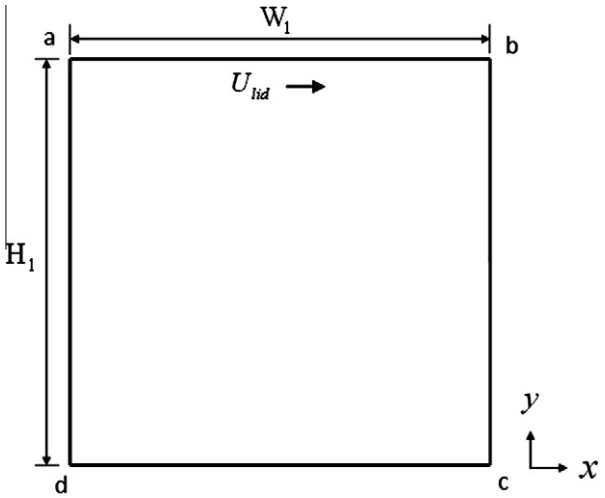


**Fig. 1.** Schematic diagram of the lid-driven flow.

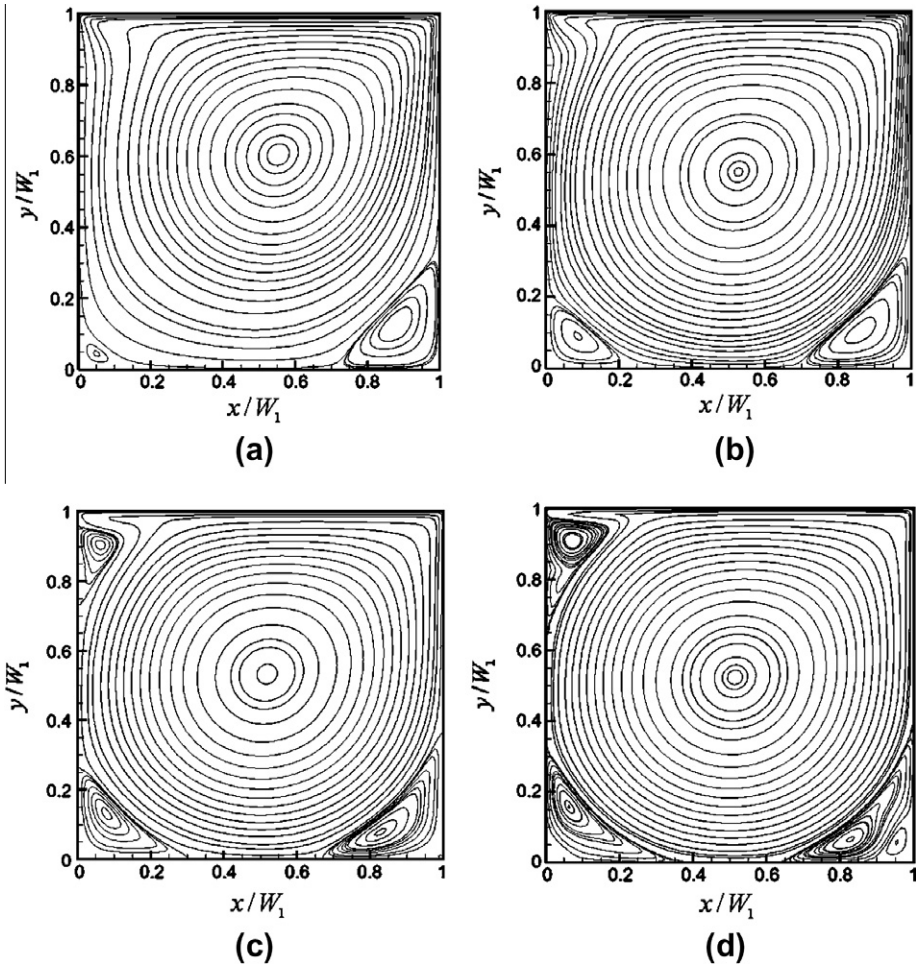


**Fig. 2.** Streamlines of lid-driven flow with Re=(a) 400, (b) 1000, (c) 5000, and (c) 10000.

increasing the height of central fins in the radiator appropriately. The present study focuses on the heat transfer phenomena of impinging jet flows in a channel. As a benchmark, the closed lid-driven cavity flow and open backward-facing step flow are simulated first in this paper and compared with experimental data. Subsequently, the analysis of transient jet impingement is carried out with various physical parameters. Both constant temperature and constant heat flux boundaries are considered in the turbulent impinging jet under high Reynolds number (Re).

## 2. Mathematical model

The two-dimensional turbulent flow is assumed to be incompressible, have a constant viscosity, and to be under negligible gravity conditions. The vorticity-streamfunction-based governing equations [13] and energy equation for heat transfer are described as following.

### 2.1. LBM-like algorithm for vorticity function

The vorticity function is

$$\frac{\partial\omega}{\partial t}+u\frac{\partial\omega}{\partial x}+v\frac{\partial\omega}{\partial y}=\frac{\partial}{\partial x}\left(\upsilon_e\frac{\partial\omega}{\partial x}\right)+\frac{\partial}{\partial y}\left(\upsilon_e\frac{\partial\omega}{\partial y}\right), \tag{1}$$

in which the effective viscosity is calculated as

$$\upsilon_e=\upsilon_0+\upsilon_t, \tag{2}$$

where $\upsilon_0 = 1/Re$. The eddy viscosity $\upsilon_t$ is given by the Smagorinsky model as [7]

$$\upsilon_t=(C\Delta)^2|\bar{S}|. \tag{3}$$

The LBM-like algorithm of Eq. (1) with a uniform lattice and the BGK collision model can be expressed as [13]

$$g_k(\vec{x}+c\vec{e}_k\Delta t,t+\Delta t)-g_k(\vec{x},t)=-\tau_e^{-1}\left[g_k(\vec{x},t)-g_k^{(eq)}(\vec{x},t)\right], \tag{4}$$

where $\mathbf{e}_k$ is the particle velocity, $g_k$ is the particle distribution function of vorticity, and $\tau_e$ is the dimensionless relaxation time related to equilibrium. For the present two-dimensional application, the D2Q5 model is adopted. The discrete velocities in this model are defined as

$$\vec{e}_k=\begin{cases}(0,0):k=0\\(\cos(k-1)\pi/2,\sin(k-1)\pi/2):k=1,2,3,4\end{cases}. \tag{5}$$

The equilibrium distribution function is

$$g_k^{(eq)}=\frac{\omega}{5}\left[1+2.5\frac{\vec{e}_k\cdot\vec{u}}{c}\right], \tag{6}$$

where $c = \Delta x/\Delta t = \Delta y/\Delta t$ is the lattice speed with relation to grid spacing $\Delta x$ and $\Delta y$ in the $x$- and $y$- directions respectively and the discrete time step, $\Delta t$. The dimensionless relaxation time is determined using

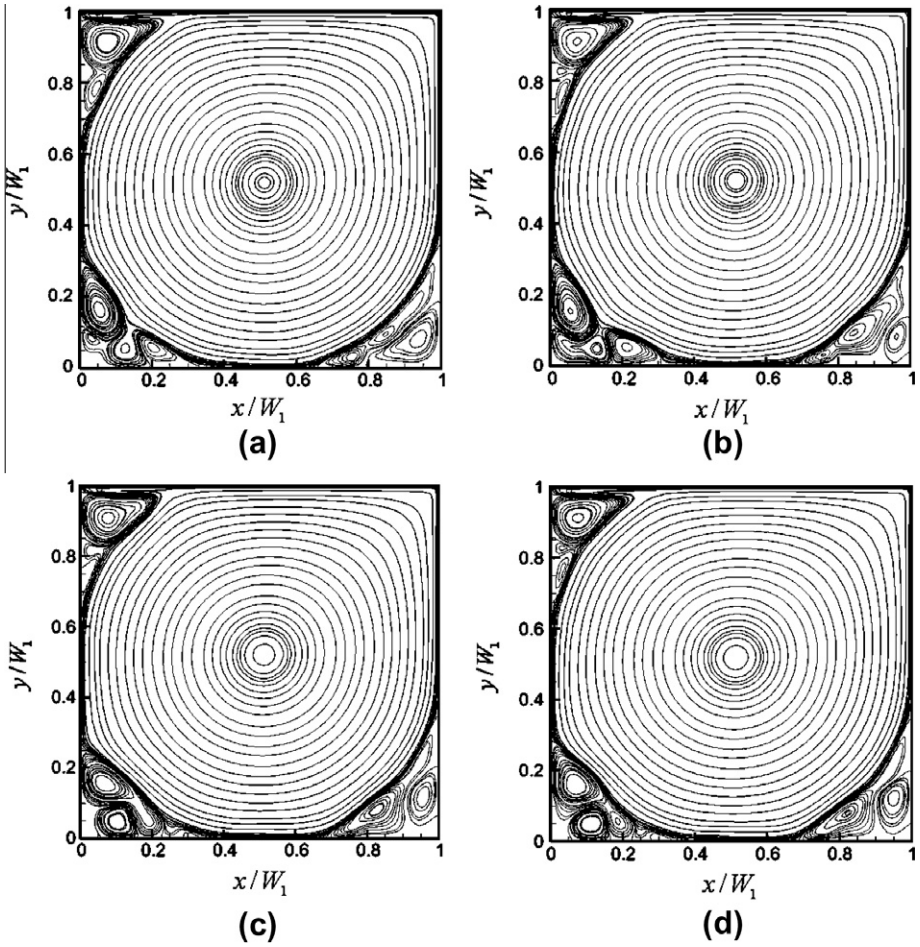


**Fig. 3.** Instantaneous streamlines of turbulent lid-driven flow with Re = 20000. (a) $t = 3*10^5\cdot\Delta t$; (b) $t = 4*10^5\cdot\Delta t$; (c) $t = 5*10^5\cdot\Delta t$; (d) $t = 5.3*10^5\cdot\Delta t$.

**Table 1**
Central location of vortices of lid-driven square cavity flow. $(x_c,y_c)$: primary vortex; $(x_l,y_l)$: lower left vortex; $(x_r,y_r)$: lower right vortex.

| Re | | $x_c$ | $y_c$ | $x_l$ | $y_l$ | $x_r$ | $y_r$ |
|---|---|---|---|---|---|---|---|
| 400 | Chen [13] | 0.5500 | 0.6125 | 0.0625 | 0.0501 | 0.8820 | 0.1250 |
| | Present work | 0.5621 | 0.6300 | 0.0600 | 0.0526 | 0.8910 | 0.1176 |
| 1000 | Chen [13] | 0.5310 | 0.5700 | 0.0901 | 0.0800 | 0.8501 | 0.1100 |
| | Present work | 0.5313 | 0.5680 | 0.0876 | 0.0811 | 0.8523 | 0.1137 |
| 5000 | Chen [13] | 0.5040 | 0.5001 | 0.0950 | 0.1100 | 0.8285 | 0.0745 |
| | Present work | 0.5101 | 0.5034 | 0.1032 | 0.1084 | 0.8089 | 0.0733 |
| 10000 | Chen [13] | 0.5117 | 0.5313 | 0.0585 | 0.1655 | 0.7813 | 0.0625 |
| | Present work | 0.5111 | 0.5313 | 0.0580 | 0.1655 | 0.8003 | 0.0642 |
| 20000 | Chen [13] | 0.5078 | 0.5313 | – | – | – | – |
| | Present work | 0.5078 | 0.5325 | – | – | – | – |

$$\tau_e = \frac{1}{C_s^2 Re\Delta t} + 0.5 + \frac{(C\Delta)^2|\bar{S}|}{C_s^2\Delta t}, \tag{7}$$

where the speed of sound $C_s$ is defined as

$$C_s^2 = \frac{2}{5}c^2. \tag{8}$$

The calculation of the strain rate can be derived as [13]

$$|\bar{S}| = \sqrt{2S_{\alpha\beta}S_{\alpha\beta}} = |\omega|. \tag{9}$$

### 2.2. LBM-like algorithm for stream function

The stream function equation is

$$\frac{\partial^2\psi}{\partial x^2} + \frac{\partial^2\psi}{\partial y^2} = -\omega. \tag{10}$$

The LBM evolution equation of stream function with a uniform lattice and the BGK collision model can be expressed as [13]

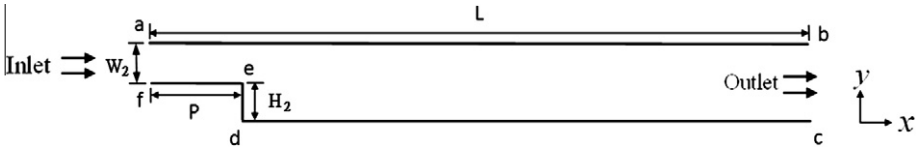


**Fig. 4.** Schematic diagram of the backward-facing step flow.

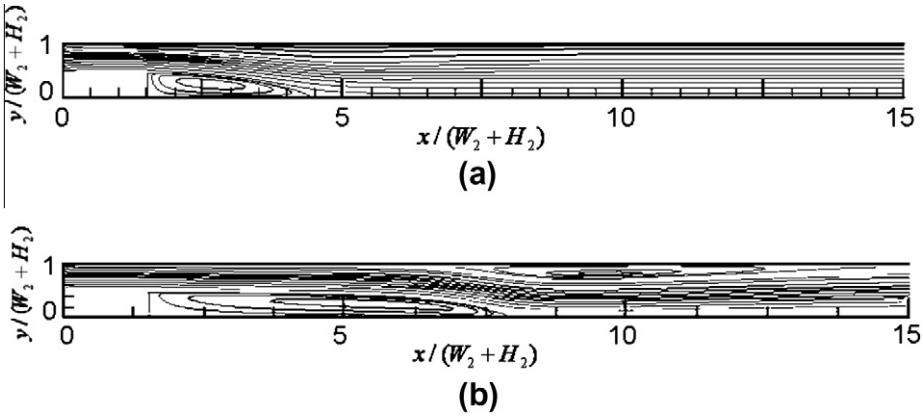


**Fig. 5.** Streamlines of backward-facing step flow with Re = (a) 300 and (b) 1500.

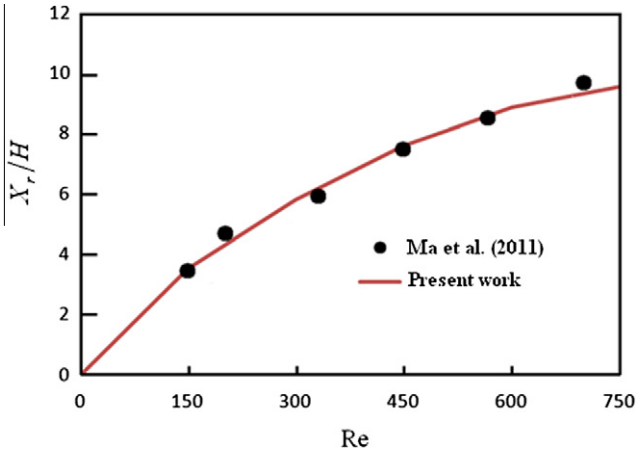


**Fig. 6.** Reattachment point of the backward-facing step flow related to different Re.

$$f_k(\vec{x}+c\vec{e}_k\Delta t, t+\Delta t) - f_k(\vec{x},t) = \Omega_k + \Omega'_k, \tag{11}$$

where

$$\Omega_k = -\frac{1}{\tau_\psi}\left[f_k(\vec{x},t) - f_k^{(eq)}(\vec{x},t)\right], \tag{12}$$

$$\Omega'_k = \Delta t\zeta_k(-\omega)D. \tag{13}$$

$f_i$ is the particle distribution function of stream function. The artificial diffusion coefficient $D$ is expressed as

$$D = \frac{c^2}{2}\left(\frac{1}{2} - \tau_\psi\right). \tag{14}$$

The relaxation time of the stream function, $\tau_\psi$, can be chosen arbitrarily above 0.5. The lattice model is the same as in the vorticity model. The equilibrium distribution function in Eq. (12) is

$$f_k^{(eq)}(\vec{x},t) = \begin{cases} (\xi_0 - 1)\psi(\vec{x},t), & k = 0, \\ \xi_k\psi(\vec{x},t), & k = 1,2,3,4. \end{cases} \tag{15}$$

The weight parameters $\zeta_k$ and $\xi_k$ are defined as

$$\sum_{k=0}^{4}\zeta_k = 1, \tag{16}$$

$$\sum_{k=0}^{4}\xi_k = 1, \tag{17}$$

which give

$$\xi_0 = 0, \xi_1 = \xi_2 = \xi_3 = \xi_4 = \frac{1}{4}, \tag{18}$$

$$\xi_0 = 0, \xi_1 = \xi_2 = \xi_3 = \xi_4 = \frac{1}{4}. \tag{19}$$

$\psi$is obtained as

$$\psi(\vec{x},t) = \frac{1}{1-\xi_0}\sum_{k=1}^{4} f_k \tag{20}$$

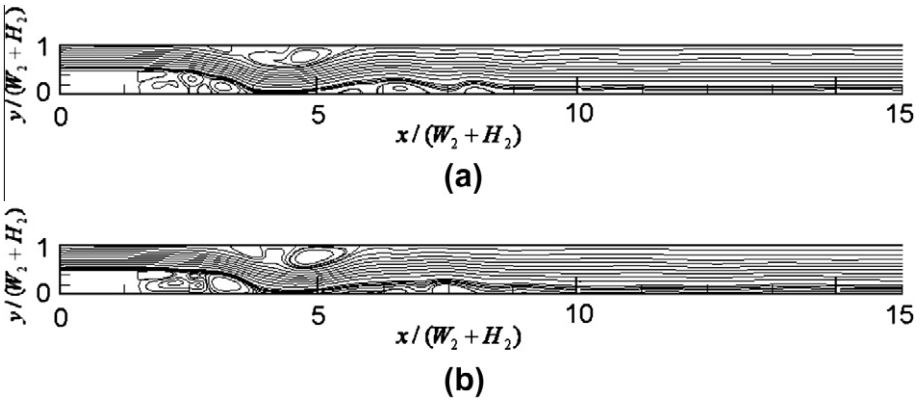


**Fig. 7.** Instantaneous streamlines of turbulent backward-facing step flow with Re = 2400. (a) $t = 1.5{*}10^5{\cdot}\Delta t$; (d) $t = 3{*}10^5{\cdot}\Delta t$.

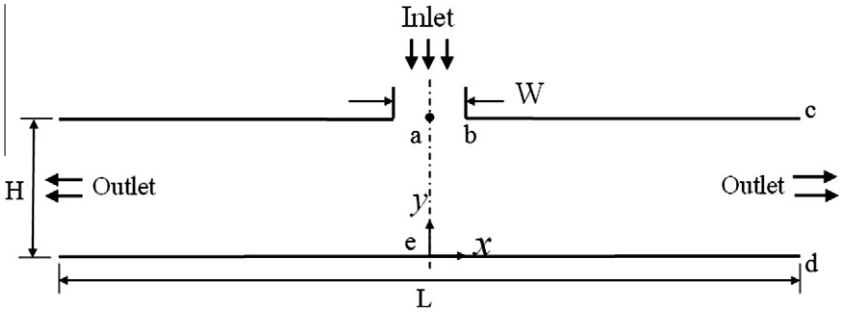


**Fig. 8.** Schematic diagram of impinging jet flow.

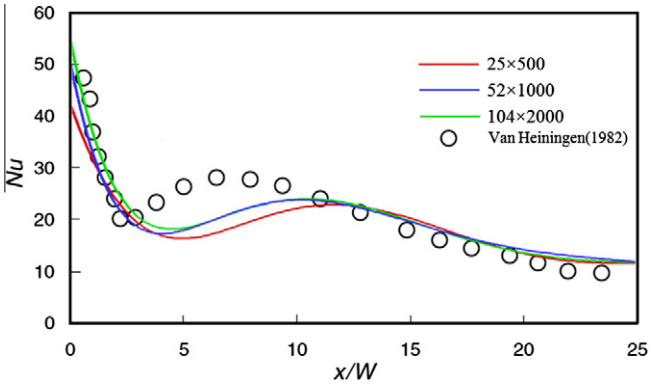


**Fig. 9.** Local Nu distribution on the impingement surface under constant-temperature condition. (H/W = 2.6, Re = 10200).

### 2.3. LBM-like algorithm for energy equation

The energy equation is

$$\frac{\partial T}{\partial t}+u\frac{\partial T}{\partial x}+v\frac{\partial T}{\partial y}=\frac{\partial}{\partial x}\left(\alpha_e\frac{\partial T}{\partial x}\right)+\frac{\partial}{\partial y}\left(\alpha_e\frac{\partial T}{\partial y}\right), \tag{21}$$

in which the effective diffusion coefficient is calculated as

$$\alpha_e=\alpha_0+\alpha_t, \tag{22}$$

where

$$\alpha_0=\frac{1}{Re\Pr}, \tag{23}$$

$$\alpha_t=\frac{(C\Delta)^2|\bar{S}|}{\Pr_T}. \tag{24}$$

In this work, we develop a similar LBM-like algorithm to energy equation as for the models of vorticity and stream function in Chen's work [13]. The evolution equation is expressed as

$$h_k(\vec{x}+c\vec{e}_k\Delta t,t+\Delta t)-h_k(\vec{x},t)=-\tau_T^{-1}\left[h_k(\vec{x},t)-h_k^{(eq)}(\vec{x},t)\right] \tag{25}$$

where $h_k$ is the particle distribution function. The equilibrium distribution function is calculated as

$$h_k^{(eq)}=\frac{T}{5}\left[1+2.5\frac{\vec{e}_k\cdot\vec{u}}{c}\right]. \tag{26}$$

The lattice model is the same as described above. The dimensionless relaxation time is determined using

$$\tau_T=\frac{1}{C_s^2Re\Pr\Delta t}+0.5+\frac{(C\Delta)^2|\bar{S}|}{C_s^2\Pr_T\Delta t}. \tag{27}$$

### 2.4. Simulation parameters

The dynamical similarity of the impinging jet depends on the Reynolds number and the Prandtl number, while convective heat transfer depends on the Nusselt number. These dimensionless parameters are defined as

$$Re=\frac{V_{in}W}{\upsilon}, \tag{28}$$

$$\Pr=\frac{\upsilon}{\alpha}, \tag{29}$$

$$Nu=-\frac{W}{T_w-T_{in}}\frac{\partial T}{\partial n}. \tag{30}$$

In the present LBM model, the boundary conditions are easy to be implemented according to the equilibrium distribution function of given physical conditions. The simulations are terminated in accordance with the following convergence criteria as

$$\frac{|\omega(x,y,t+\Delta t)-\omega(x,y,t)|}{|\omega(x,y,t)|}\leqslant 10^{-5}, \tag{31}$$

$$\frac{|\psi(x,y,t+\Delta t)-\psi(x,y,t)|}{|\psi(x,y,t)|}\leqslant 10^{-6}, \tag{32}$$

$$\frac{|T(x,y,t+\Delta t)-T(x,y,t)|}{|T(x,y,t)|}\leqslant 10^{-5}. \tag{33}$$

Since the turbulence is a transient phenomenon, the convergence achievement is determined when the residue is varied in a small and steady range. In order to capture the unsteady flow phenomena in turbulence, the time average of turbulent physical quantity is evaluated.

## 3. Results and discussion

The large-eddy-based lattice Boltzmann model with the effective viscosity and diffusion coefficient is applied in hydrodynamic and thermal simulations whether the flow is turbulent or not. But in laminar cases, the values of eddy terms are practically insignificant and have no contribution to flow phenomena.

### 3.1. Closed lid-driven flow and open backward-facing step flow

Based on the model of vorticity and steam function, the closed lid-driven flow was simulated first and compared with Chen's results [13]. All quantities are nondimensionalized by the grid length, lattice speed, and reference temperature so that the value of dimensionless grid length, time step, and lattice speed is unity [1]. Fig. 1 shows the simulation model of the lid-driven flow. The grid resolution is $128\times128$ for grid independence. The no-slip condition is applied on all walls except the top lid moving with $u=u_{lid}, v=0$. The stream boundary on all walls are $\psi=0$ and $\frac{\partial\psi}{\partial n}=0$, in which $n$ means the normal direction of the wall. The values of $\omega$ on the stationary walls are calculated by Chen et al. [23]

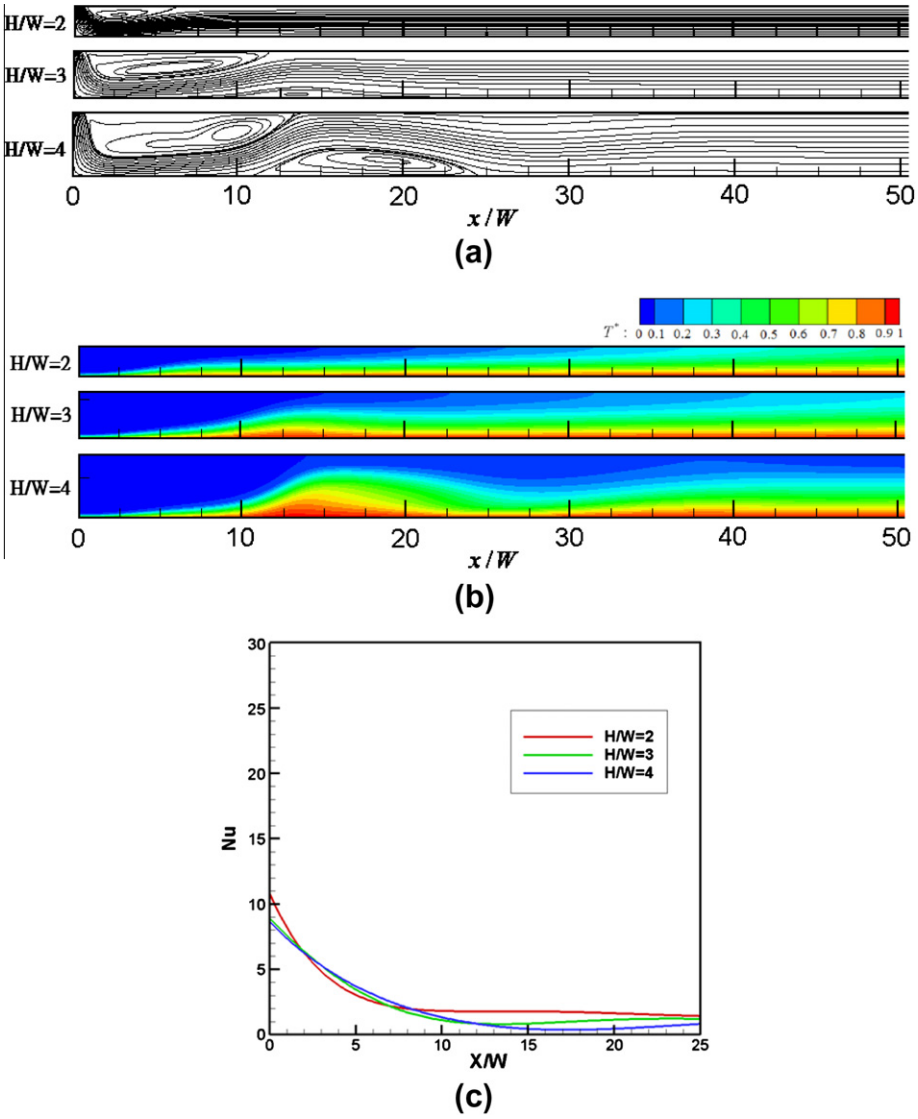


**Fig. 10.** (a) Streamlines, (b) temperature contours $\left(T^* = \frac{T-T_{in}}{T_w-T_{in}}\right)$ and (c) local Nu distributions on the isothermal surface of impinging jet flow with Re = 300 in channels of different H/W. All flows are laminar.

$$\omega_{i,1} = \frac{7\psi_{i,1} - 8\psi_{i,2} + \psi_{i,3}}{2\Delta n^2}, \tag{34}$$

while those on the moving lid are calculated by

$$\omega_{i,1} = \frac{7\psi_{i,1} - 8\psi_{i,2} + \psi_{i,3}}{2\Delta n^2} - \frac{3U_{lid}}{\Delta n}. \tag{35}$$

The Reynolds number is defined as $\frac{U_{lid}W_1}{\nu}$.

Fig. 2 shows the streamlines of the lid-driven flow with Re from 400 to 10,000. A primary vortex is found in the center of the cavity accompanied with small vortices appear in the lower right, lower left, and top left corner in turn as Re increased. In the case of Re = 10,000, the flow field is in the region of transitional flow, and a small vortex is produced behind the vortex of the lower right corner. As Re reaches to 20,000, only the primary vortex is located at a steady position. In Fig. 3, the transient turbulent flow field of Re = 20,000 shows the other vortices in corners are disturbed. The central locations of vortices of the lid-driven square cavity flow with different Re are listed in Table 1 and in good agreement with Chen's results [13].

Since Chen's work [13] focused on the lid-driven flow, the feasibility of this LBM model for an open flow field should be validated. In this study, simulation results of the backward-facing step flow was concerned and compared with other works. The simulation model is shown in Fig. 4. The boundary conditions of inlet are $u = U_{in}, v = 0, \psi = \int_0^{W_2} U_{in}dy$ and $\omega = 0$, while those of outlet are $\frac{\partial\omega}{\partial x} = 0$ and $\frac{\partial\psi}{\partial x} = 0$. All walls are stationary with the same boundary conditions as in the lid-driven flow except the top wall with stream boundary of $\psi = U_{in} \cdot W_2$. The Reynolds number is defined as $\frac{U_{in}(W_2+H_2)}{\nu}$ in this case.

Fig. 5 shows the streamlines of flows with Re = 300 and 1500. A primary vortex is found behind the step with the position of reattachment point moving backwards further as Re increased. The position of reattachment point is in good agreement with the results of Ma et al. [24], as shown in Fig. 6. The results also show that another vortex is observed near the top wall if the Re is high enough, as in the case of Re = 1500 in Fig. 5(b). In regard to a higher Re of 2400, the flow field is transformed from laminar flow to turbulence. The instantaneous streamlines in Fig. 7 show that several transient vortices are produced both near top and bottom walls.

The results in this section demonstrate the extensive applicability of Chen's method [13] on both closed and open flow systems without respect to laminar flow or turbulence. In the following sections, we applied this method to investigate the impinging jet flows. The thermal LBM model in Section 2.3 was also introduced to study the transient heat transfer phenomena.

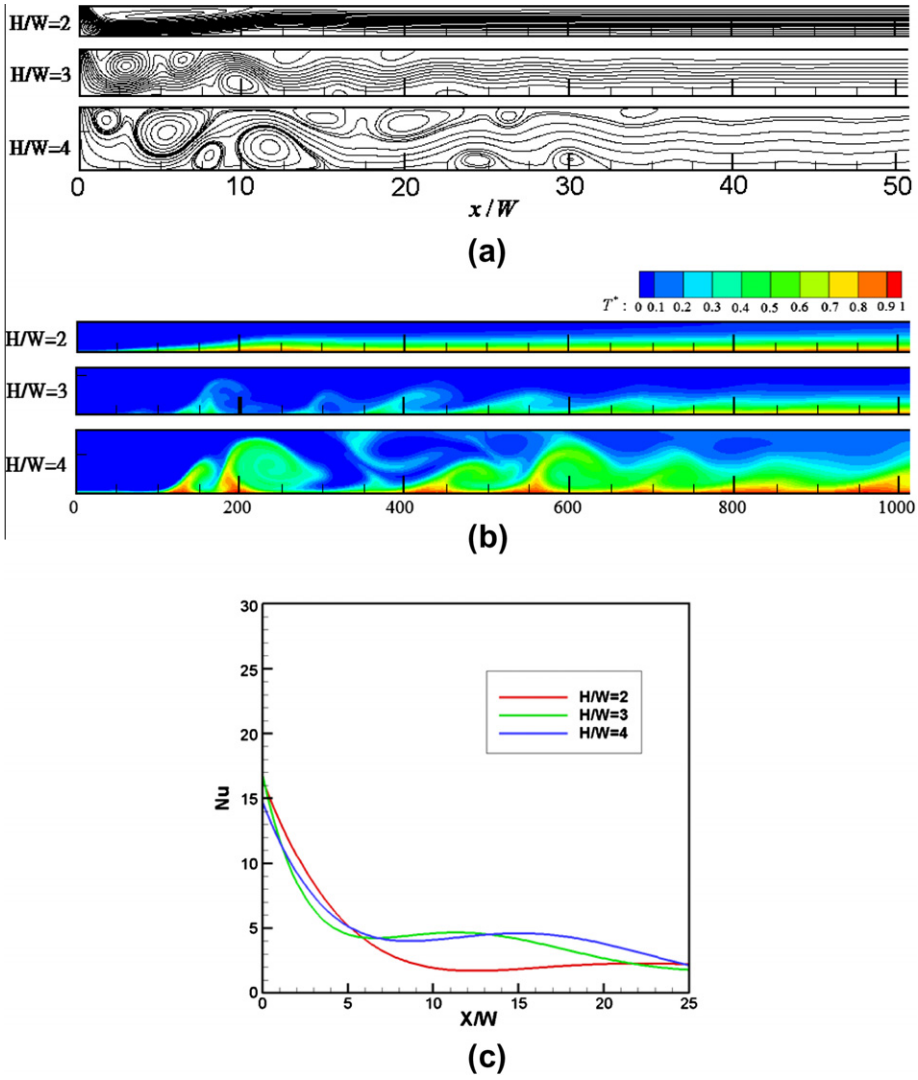


**Fig. 11.** (a) Streamlines, (b) temperature contours $\left(T^* = \frac{T-T_{in}}{T_w-T_{in}}\right)$ and (c) local Nu distributions on the isothermal surface of impinging jet flow with Re = 800 in channels of different H/W. Case of H/W = 2 is laminar flow while others are turbulence.

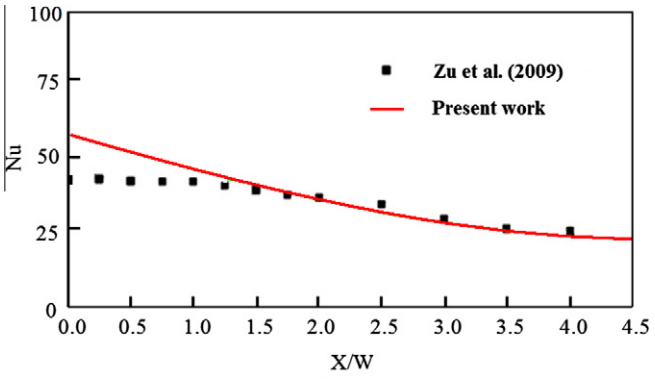


**Fig. 12.** Local Nu distribution on the impingement surface under constant-heat-flux condition. (H/W = 2, Re = 10000).

### 3.2. Impinging jet flow on an isothermal surface

The simulation model of impinging jet flow is shown in Fig. 8. To simplify the calculation, the symmetric boundary (a–e) is used. A uniform flow with constant temperature from inlet (a,b) is impinged on the bottom surface (d,e), which is supposed to be isothermal in this section. As in the backward-facing step flow, all walls are no-slip and the outlet (c,d) has fully developed flow in a distance away from the inlet enough. To focus on the cooling effect of the impinging jet flow on the hot bottom surface, the top wall (b,c) is treated as adiabatic.

The impinging jet flow with Re = 10200 is simulated and compared with the experimental results of Van Heiningen [25] for validation. Three grid sizes for coarse ($W = 10\Delta x$), medium ($W = 20\Delta x$) and fine ($W = 40\Delta x$) mesh are considered here to ensure the simulation results are grid independent. The results shown in Fig. 9 are in good agreement with Van Heiningen's data [25] except for the region between X/W = 5 to 10. Sharif and Mothe [19] indicated that in this case, the impinging plate is within the region of the jet potential core, where the flow is essentially laminar. Therefore, their numerical results by several turbulence models presented the same inaccuracy near the jet exit. After the impingement, the laminar-to-turbulent transition occurs downstream in the wall jet region, and this causes the second peak of local Nusselt number distribution in the experimental results. In Sharif and Mothe's work [19], this peak was not captured by any of the turbulence models used. Since the present method can characterize not only laminar but also turbulent flows well, the second

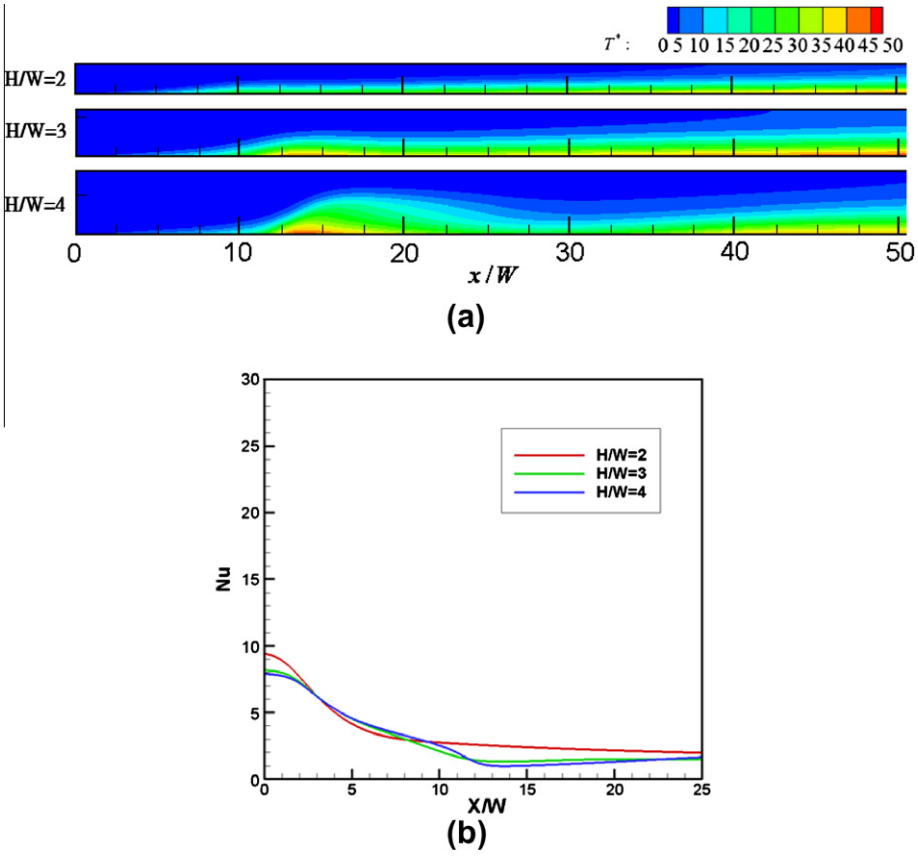


**Fig. 13.** (a) Temperature contours $\left(T^* = \frac{T-T_{in}}{q_0 \Delta x / k_f}\right)$ and (b) local Nu distributions on a surface under constant-heat-flux condition of impinging jet flows. Other boundary conditions are the same as in Fig. 10.

peak is observed in this study, as shown in Fig. 9. In the subsequent discussion, the medium grid size of simulations is adopted in the cause of both accuracy and efficiency.

To investigate the influence of the ratio of jet-to-surface distance to jet exit width, three cases of H/W = 2, 3 and 4 are discussed. The results of Re = 300 in Fig. 10 present laminar flows in all cases. As the channel size increased, the vortices near walls are enlarged. Inspecting the temperature contours and local Nu distributions on the bottom surface, it is found that the expanded vortices cause a great influence on the surface cooling. The stationary vortex in the laminar flow field constrains the heat diffusibility, and hence forms a local high-temperature zone. Therefore, the convective heat transfer of the laminar impinging jet flow in a narrow channel is better that that in a wide channel.

As the Re increasing, the flow field related to high H/W might be transformed into turbulence, while the case of low H/W with same Re still has laminar flow. Fig. 11 shows an illustration of Re = 800. In the case of H/W = 3, the fluid flow in the region near the jet exit is turbulent, while the downstream area is laminar as in the case of H/W = 2. As H/W increasing to 4, the turbulent region is expanded. Comparing with the results of laminar flows, although more transient vortices are produced in the turbulence, they are not stationary. The temperature contours show that the heat can be carried from the bottom surface to top wall by the moving vortices. The local Nu distributions in Fig. 11(c) reveal that these turbulent transport phenomena can enhance the convective heat transfer of impinging jet flow substantially.

The results in the present work show that the critical Reynolds number for a laminar flow transforming into turbulence is depended on the ratio of jet-to-surface distance to jet inlet width. For an impinging jet flow under the laminar region, a small H/W is preferred for a better cooling efficiency. However, for the turbulent jet flow, a sufficient space to produce transient moving vortices, which have great contribution to convective heat transfer, is proposed.

### 3.3. Impinging jet flow on a surface under constant-heat-flux condition

In this section, the impingement surface of a constant-heat-flux boundary condition is taken into account. For the jet flow of Re = 10,000 in a channel with H/W = 2, the local Nu distribution on the heating surface is in good agreement with the results of Zu et al. [18], as shown in Fig. 12. In regard to the cases of Fig. 10, similar results are obtained. Fig. 13 shows that in the case of H/W = 2, the energy is transported from heating surface to the flow, and causes a hotter fluid downstream than upstream. But in the case of high H/W, the stationary vortex near the heating surface constrains the heat transfer with fluid. Therefore, fluid with high local temperature is observed upstream. The tendency of local convective heat transfer in laminar impinging jet flow on the surface under constant-heat-flux condition is similar to that under constant-temperature condition, as shown in Fig. 13(b).

The turbulent jet flows of Re = 800 on the surface under constant-heat-flux condition are shown in Fig. 14. Because the heat transfer efficiency is enhanced by transient vortices, the fluid heating phenomena are weaker than that of a laminar flow. The maximum downstream temperature of the turbulent flow is smaller than that of a laminar flow with the same Reynolds number, and no high-temperature zone appears upstream. Otherwise, unlike the results in Fig. 11(b), the temperature contours of Fig. 14 show that the heat is rarely transported to the top wall. The distribution of local Nu reveals that the tendency of convective heat transfer in turbulent impinging jet flow is similar to that under constant-temperature condition. For a surface under these two boundary

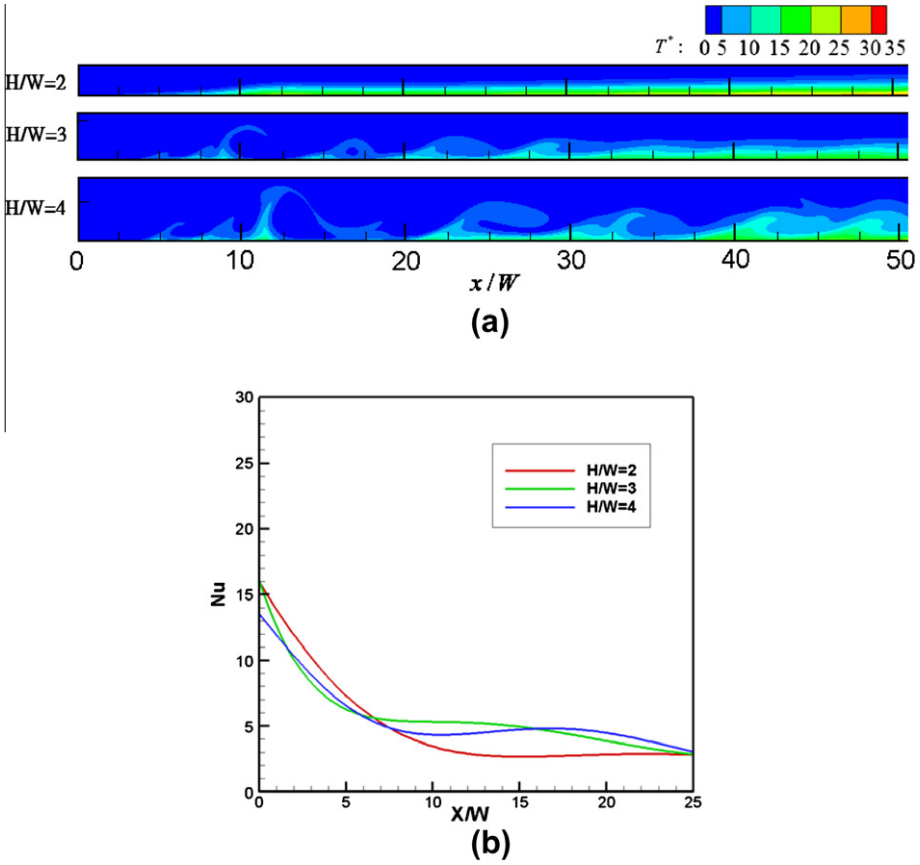


**Fig. 14.** (a) Temperature contours $\left(T^* = \frac{T-T_{in}}{q_0 \Delta x / k_f}\right)$ and (b) local Nu distributions on a surface under constant-heat-flux condition of impinging jet flows. Other boundary conditions are the same as in Fig. 11.

conditions, the results show that Nu is raised with increasing jet Reynolds number.

## 4. Conclusion

This study used the LBM combined with LES to simulate impinging jet flow for surface cooling. Three LBM-like algorithms for vorticity, stream function and energy equations are developed to simulate the transport phenomena of laminar and turbulent flow fields. To verify the present method is feasible for both a closed and open flow field, the lid-driven flow and backward-facing flow are simulated and compared with other data. The results present good accuracy on the vortex locations of the lid-driven flow and the reattachment point of the backward-facing step flow. For the impinging jet flow on an isothermal surface, the result of convective heat transfer is in good agreement with experimental data, especially in capturing the second peak of local Nusselt number distribution, which is caused by the laminar-to-turbulent transition after the impingement.

For surface cooling by impinging jet flow, the ratio of jet-to-surface distance to jet exit width, H/W, is very important. The present work shows that if the height of the impact of the jet is changed, the Reynolds number required achieving turbulence changes, i.e. the turbulent flow is easier to achieve with a high impact. In the laminar jet flow, stationary vortices are produced near the hot surface and reduce the heat transfer effect. Therefore, a small H/W, which suppresses the vortex size, can cause a better cooling efficiency. But in the turbulent jet flow, the transient moving vortices can carry the energy from hot surface into the fluid rapidly. Consequently, high H/W for producing more transient moving vortices is preferred. Otherwise, the impinging jet cooling on the surface under constant-temperature or constant-heat-flux condition is discussed simultaneously and gets similar results.

## Acknowledgements

This study acknowledges the support provided to this research by the National Science Council of Republic of China under Grant No. NSC 98-2221-E-006-167.

## References

[1] D.W. Gladrow, Lattice-Gas Cellular Automata and Lattice Boltzmann Models: An Introduction, Springer, 2000.
[2] S. Succi, The lattice Boltzmann equation, Oxford University Press, 2001.
[3] J. Zhang, Lattice Boltzmann method for microfluidics: models and applications, Microfluid. Nanofluid. 10 (1) (2011) 1–28.
[4] G.R. McNamara, G. Zanetti, Use of the Boltzmann equation to simulate lattice-gas automata, Phys. Rev. Lett. 61 (20) (1998) 2332–2335.
[5] P.L. Bhatnagar, E.P. Gross, M. Krook, A model for collision process in gases. I. Small amplitude processes in charged and neutral one component system, Phys. Rev. 94 (3) (1954) 511–521.
[6] S.C. Chang, Y.S. Hsu, C.L. Chen, Lattice Boltzmann simulation of fluid flows with fractal geometry: an unknown-index algorithm, J. Chinese Soc. Mech. Eng. 32 (6) (2011) 523–531.
[7] J.S. Smagorinsky, General circulation experiments with the primitive equation I. The basic experiment, Mon. Weather Rev. 91 (1963) 99–164.
[8] J.W. Deardorff, A numerical study of 3 dimensional turbulent channel flow at large Reynolds number, J. Fluid Mech. 41 (1970) 453–480.
[9] W.W. Kim, S. Menon, H.C. Mongia, Large eddy simulation of a gas turbine combustor flow, Combust. Sci. Technol. 143 (1999) 25–62.
[10] X. Zhou, K.H. Luo, J.J.R. Williams, Study of density effects in turbulent buoyant jets using large-eddy simulation, Theor. Comput. Fluid Dyn. 15 (2) (2001) 95–120.
[11] G. Yu, E.J. Avital, J.J.R. William, Large eddy simulation of flow past free surface piercing circular cylinders, J. Fluids Eng. – Trans. ASME 130 (10) (2008) 101304.

[12] S.M. Hashemian, M. Rahnama, M. Farhadi, Large eddy simulation of turbulent heat transfer in a channel with a square cylinder, Heat Transfer Eng. 33 (12) (2012) 1052–1062.
[13] S. Chen, A large-eddy-based lattice Boltzmann model for turbulent flow simulation, Appl. Math. Comput. 215 (2) (2009) 591–598.
[14] R.K. Agarwal, W.W. Bower, Navier–Stokes computations of turbulent compressible two-dimensional impinging jet flowfields, AIAA J. 20 (5) (1982) 577–584.
[15] J.G. Maveety, J.F. Hendricks, A heat sink performance study considering material, geometry, nozzle placement, and Reynolds number with air impingement, J. Electron. Packag. 121 (3) (1999) 56–161.
[16] Y.L. Shi, M.B. Ray, A.S. Mujumdar, Computational study of impingement heat transfer under a turbulent slot jet, Ind. Eng. Chem. Res. 41 (18) (2002) 4643–4651.
[17] S.J. Wang, A.S. Mujumdar, A comparative study of five low Reynolds number $k-\varepsilon$ models for impingement heat transfer, Appl. Therm. Eng. 25 (1) (2005) 31–44.
[18] Y.Q. Zu, Y.Y. Yan, J. Maltson, Numerical study on stagnation point heat transfer by jet impingement in a confined narrow gap, J. Heat Transfer – Trans. ASME 131 (2009) 094504.
[19] M.A.R. Sharif, K.K. Mothe, Evaluation of turbulence models in the prediction of heat transfer due to slot jet impingement on plane and concave surfaces, Numer. Heat Transfer Part B: Fundam. 55 (4) (2009) 273–294.
[20] A.C. Benim, K. Ozkan, M. Cagan, D. Gunes, Computational investigation of turbulent jet impinging onto rotating disk, Int. J. Numer. Methods Heat Fluid Flow 17 (3) (2007) 284–301.
[21] H.M. Hofmann, R. Kaiser, M. Kind, H. Martin, Calculation of steady and pulsating impinging – an assessment of 13 widely used turbulence models, Numer. Heat Transfer Part B: Fundam. 51 (6) (2007) 565–583.
[22] Y.T. Yang, H.S. Peng, Numerical study of pin-fin heat sink with un-uniform fin height design, Int. J. Heat Mass Transfer 51 (19–20) (2008) 4788–4796.
[23] S. Chen, J. Tölke, M. Krafczyk, A new method for the numerical solution of vorticity-streamfunction formulations, Comput. Methods Appl. Mech. Eng. 198 (3-4) (2008) 367–376.
[24] K. Ma, W.L. Wei, L.L. Wang, X.J. Zhao, Large eddy numerical simulation of flows over a backward-facing step, in: International Symposium on Water Resource and Environmental Protection (ISWREP), vol. 4, 2011, pp. 3024–3026.
[25] A.R.P. Van Heiningen, Heat transfer under an impinging slot jet, Ph.D. thesis, McGill University, Montreal, Quebec, Canada, 1982.